

# Transient scaling and resurgence of chimera states in coupled Boolean phase oscillators

David P. Rosin,<sup>1,2</sup> Damien Rontani,<sup>1,3</sup> Nicholas D. Haynes,<sup>1</sup> Eckehard Schöll,<sup>2</sup> and Daniel J. Gauthier<sup>1</sup>

<sup>1</sup>*Department of Physics, Duke University, 120 Science Drive, Durham NC 27708, USA*

<sup>2</sup>*Institut für Theoretische Physik, Technische Universität Berlin, Hardenbergstr. 36, Berlin D-10623, Germany*

<sup>3</sup>*Supélec, OPTEL research group and LMOPS EA-4423, 2 Rue Edouard Belin, Metz F-57070, France*

(Dated: March 21, 2022)

We study experimentally and theoretically the dynamics of networks of non-locally coupled electronic oscillators that are described by a Kuramoto-like model. The experimental networks show long complex transients from random initial conditions on the route to network synchronization. The transients display complex behaviors, including resurgence of chimera states, which are network dynamics where order and disorder coexists. The spatial domain of the chimera state moves around the network and alternates with desynchronized dynamics. The fast timescale of our oscillators (on the order of 100 ns) allows us to study the scaling of the transient time of large networks of more than a hundred nodes. We find that the average transient time increases exponentially with the network size and can be modeled as a Poisson process. This exponential scaling is a result of a synchronization rate that follows a power law of the phase-space volume.

As discovered recently, the dynamical state of networks can show a surprising behavior, where network nodes split into coexisting domains of entirely different dynamics, such as synchronized and unsynchronized dynamics. These so-called chimera states have been identified theoretically as long chaotic transients towards synchrony for finite-size networks, scaling exponentially with the system size [1–9]. Predicting the timescale for the transition to synchronization is crucial for many applications and is of great importance for many biological networks [10, 11]. Determining the scaling of the transient time of chimera states experimentally, however, has not been possible because of slow characteristic timescales of experimental network nodes [12–17]. Even in theoretical studies, the scaling of the transient time could only be verified in small networks of less than 45 nodes because larger networks require prohibitively long computation times [5, 18].

Here, we study the transient behavior of chimera states in an experimental network of Boolean phase oscillators realized with electronic logic circuits. Because these nodes operate on a timescale of  $\sim 100$  ns, we can study the scaling of the transient in large networks of more than a hundred nodes. The transient includes chimera states for about 14% of the time for  $N = 128$  and ends in a nearly synchronized state. We find that the transient time follows a Poisson process and that the average transient time increases exponentially with the network size, which is a result of the synchronization rate that follows a power law of the phase-space volume.

The oscillatory network nodes are realized with unclocked logic circuits together with directly-wired links on microelectronic chips, realizing an autonomous Boolean network (ABN). Besides their applications as engineered systems for random number generation and neuromorphic computation [19–21], ABNs are also a common model for genetic circuits [22–24]. The ABN studied here is a variant of all-digital phase-locked loops, which are

widely used for frequency synthesis [25, 26].

We study networks of  $N$  coupled Boolean phase oscillators as shown schematically in Fig. 1(a), where oscillator  $i \in \{1, 2, \dots, N\}$  is non-locally coupled to multiple other oscillators  $j$  in a network with a specific topology that we discuss later. To achieve coupling and oscillatory dynamics using unclocked logic gates, we implement an inverter gate with delayed feedback as shown in Fig. 1(b). This construct, for a constant delay  $\tau_i$ , is commonly known as ring oscillator [27] with a frequency given by

$$f_i = \frac{1}{2\tau_i}, \quad (1)$$

where the factor two results from inverted delayed feedback because a signal propagates through the feedback twice to reach its initial state. To implement an oscillator with an adjustable frequency, we implement a state-dependent delay  $\tau_i$  that changes in value depending on Boolean switches that are controlled by coupling signals. The coupling signals are generated by measuring the phase difference between the local oscillator and its neighbors. This coupling method has been introduced in Ref. [28] for up to two oscillators. We extend it here to allow for multiple inputs.

The state-dependent delay  $\tau_i$  of an oscillator is realized as shown in Fig. 1(c) with a constant part  $\tau_{0,i}$ , realized with 30 cascaded copier logic gates [28], and a variable part realized with XOR logic gates, Boolean switches, and short delay lines of value  $\sigma_i$ . The XOR logic gate is a simple phase detector that compares the phase of the oscillator  $x_i$  with the phase of a neighboring oscillator  $x_j$ . Its signal  $x_{j,i}^c$ , which corresponds to the phase difference between oscillators  $i$  and  $j$ , activates one of two paths in the Boolean switch: one path leads to a delay  $\sigma_i$  and the other leaves the delay unchanged, where the shorter delay is selected when a phase difference is detected. The

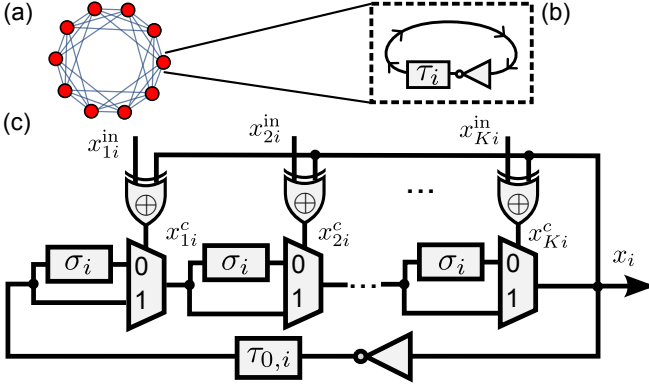


FIG. 1. (a) Illustration of a ring network with  $N = 10$  nodes and coupling range  $R = 3$ . (b) Illustration of the Boolean phase oscillator (a node in the network) consisting of an inverter gate and a state-dependent delay line  $\tau_i$ . (c) Circuit diagram of the Boolean phase oscillator showing the coupling mechanism. The rectangles, trapezoids, triangles, and shapes with  $\oplus$ -signs denote delay lines, Boolean switches (multiplexers), inverter, and XOR gates, respectively. The  $K$  coupling inputs are realized with  $K$  pairs of delay lines, multiplexers, and XOR gates, of which three are shown. The dynamical output variable is  $x_i$ .

resulting state-dependent delay is

$$\tau_i = \tau_{m,i} - \sigma_i \sum_{j=1}^K x_{ji}^c, \quad (2)$$

with maximum delay  $\tau_{m,i} = \tau_{0,i} + K\sigma_i$  and in-degree  $K$  (number of coupling inputs to the oscillator). This leads to a frequency change according to Eq. (1), resulting in coupling of oscillators and the possibility of synchronization as shown in Ref. [28].

As detailed in the supplementary material [29], Eqs. (1) and (2) can be combined to derive an approximate phase model for a network of Boolean phase oscillators

$$\dot{\phi}_i = \omega_{0,i} + \tilde{\sigma}_i \sum_{j=i-R}^{i+R} [\Theta[\sin(\phi_j)] - \Theta[\sin(\phi_i + \alpha_{ij})]], \quad (3)$$

with free-running frequencies  $\omega_{0,i}$ , coupling strengths  $\tilde{\sigma}_i$ , phase lag parameter  $\alpha_{ij}$  that results from transmission delays, and Heaviside function  $\Theta$ . The oscillators are non-locally coupled in a ring network with a coupling range  $R$  as shown schematically in Fig. 1(a). This configuration has been used previously to observe chimera states [4–8]. In the model, we assume identical oscillators ( $\omega_{0,i} = \omega_0$ ) and homogeneous coupling ( $\tilde{\sigma}_i = \tilde{\sigma}$  and  $\alpha_{ij} = \alpha$ ).

Equation (3) has a similar form as the Kuramoto model, which has been used to discover chimera states [1, 2, 5, 30]. The nonlinear coupling function in Eq. (3) differs from the sine function of phase differences in the

Kuramoto model. Because of the similarity between the two models, our network of Boolean phase oscillators is ideally suited to study chimera states experimentally.

We implement the network with electronic logic circuits on a field-programmable gate array (FPGA). The physical implementation of  $N = 128$  nodes with a coupling range  $R = 30$  requires 27,000 logic gates and 7,552 wires, which fits easily on our off-the-shelf FPGA together with a custom-built processor for data acquisition. We measure and reduce the heterogeneity in the free-running frequency of the  $N$  oscillators by adjusting the constant part of the feedback delays  $\tau_{0,i}$ , resulting in a heterogeneity of  $|\sigma_f|/\bar{f} = 0.3\%$  (average frequency  $\bar{f} = 9.14$  MHz with standard deviation  $\sigma_f = 0.03$  MHz) for  $N = 128$ . See the supplementary material [29] for technical details and sources of heterogeneity.

Implementing large networks requires us to sort the input connections to the oscillators [29], giving rise to heterogeneity in the coupling time delays whose implications are discussed later.

We first describe a particularly interesting part of the network dynamics in Fig. 2(a), showing a snapshot of the phase of oscillators in a chimera state. The oscillators outside (inside) the dotted lines, marked region I (region II), have equal (different) phases within our digitalization precision of  $\Delta\phi = \pm 0.25$  rad and hence are considered phase synchronized (desynchronized). Therefore, the oscillators in region I stay synchronized and the oscillators in region II drift apart because they have different frequencies. These frequencies are shown in Fig. 2(b) and are measured over a time period of  $6 \mu\text{s}$ , which represents approximately 60 oscillation periods. Similar to the phase picture, the oscillators in region I (region II) are frequency synchronized (desynchronized) as they have equal (different) frequencies within the digitalization precision of  $\pm 0.2$  MHz. The oscillators in region II show a regular arch shape, which is a typical spectral feature of chimera states [1, 2].

The temporal evolution of the frequency is visualized using a gray-scale image in Fig. 3(a) for a period over 7 min, corresponding to more than 4 billion oscillation periods. The figure shows that, for this specific realization, complex dynamics exist from time  $t = 0$  until  $t = 6$  min (marked III) because the frequency varies both from node to node and in time. At time  $t = 6$  min, the dynamics collapses to a nearly synchronized state (dark gray region, marked IV), where all but  $\leq 10$  oscillators have a frequency of  $f = 11.085 \pm 0.002$  MHz (compare to  $f = 9.14 \pm 0.03$  MHz for uncoupled oscillators). The remaining oscillators have a frequency different from the synchronized frequency by about 1%, which is due to heterogeneity in the experiment [29]. The time until the nearly synchronized state is reached varies considerably for different runs of the experiment. In the following, we discuss the dynamics on a microsecond timescale, at times marked in the figure.

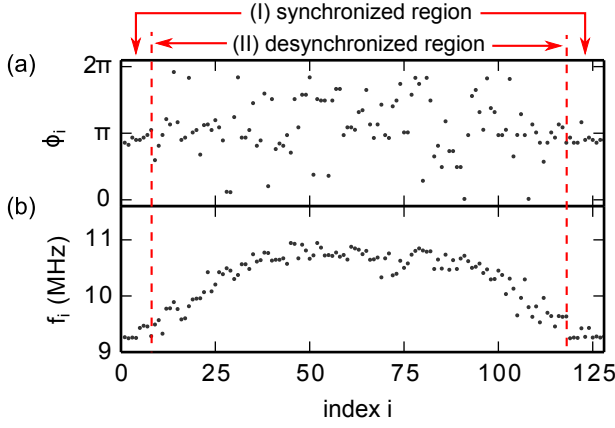


FIG. 2. Dynamics measured from coupled Boolean phase oscillators with  $N = 128$ ,  $R = 30$ ,  $\omega_0 = 2\pi(9.3 \pm 0.03)$  MHz,  $\bar{\sigma} = 2\pi(0.089 \pm 0.003)$  MHz. (a) Snapshot at  $t \approx 304$  s, (b) frequency profile  $f_i = \langle \dot{\phi}_i \rangle / (2\pi)$ . We initialize the network by first deactivating the coupling, which results in randomized initial phases because of small frequency heterogeneity, and then activating the coupling. The oscillator indices are shifted by a constant integer, so that the location of the unsynchronized domain is centered. See [29] for technical details.

Figure 3(b) shows the frequency of the Boolean phase oscillators for about 60 periods after 304 s, corresponding to a millionth of the total transient time. The network shows high frequencies (dark gray) for oscillator indices from  $i \cong 20$  to  $i \cong 100$  and low frequencies (light gray) for the remaining oscillators. This picture corresponds to the dynamics in Fig. 2(a), which we identified as a chimera state. The unsynchronized domain of the chimera (high frequency, dark gray) moves irregularly in the network, which is an effect of the finite size of the network [4, 31], and indicates that the chimera dynamics is not pinned to heterogeneities.

At an earlier time in the transient shown in Fig. 3(c), the dynamics alternates between complete desynchronization and chimera states. For times  $0 < t < 2.5 \mu\text{s}$  (marked V), the figure shows large variations in the frequencies of neighboring nodes without obvious chimera domains, corresponding to a dynamics with time intervals of both desynchronization and chimera-like states, as confirmed by analyzing the phases [29]. In the remaining part (marked VI), two domains of high and low frequencies can be identified, which correspond to a chimera state lasting over at least 30 oscillations. Again, the unsynchronized domain moves in the network. Such a disappearance and reappearance of chimera states has not been reported previously.

After a transient time  $T_N$ , the complex dynamics collapses to the synchronize state. We find that  $T_N$  varies between extreme values of  $T_{128} = 1$  s and  $T_{128} = 32$  min for 1,000 measurements, where complex dynamics are obtained for every acquisition from random initializations.

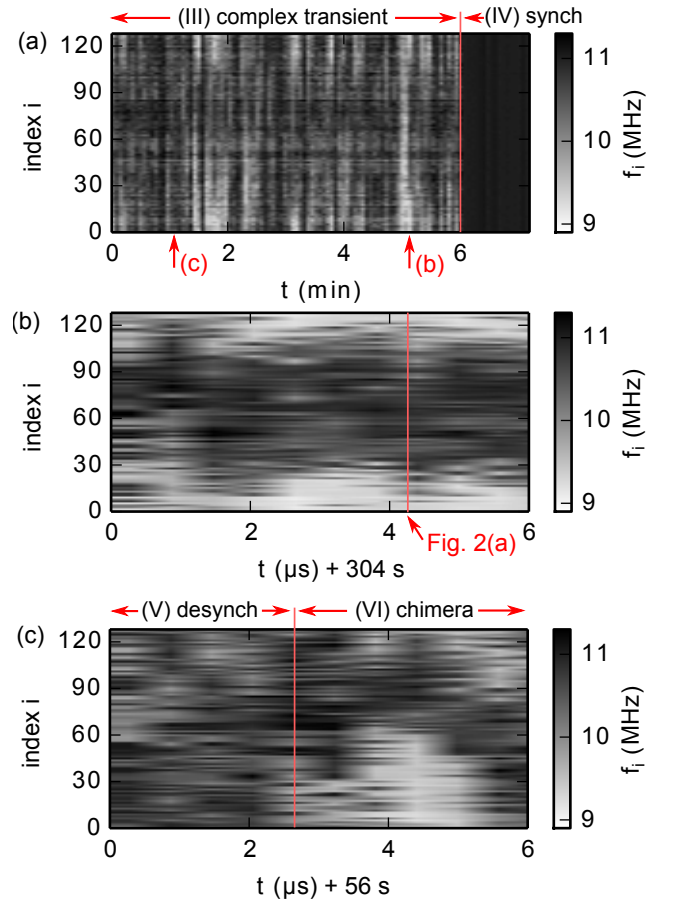


FIG. 3. (a) Frequency evolution over a time period of 7 min; averaged over  $6 \mu\text{s}$  windows (60 oscillations) every 4 s. (b), (c) Frequency evolutions shown over a time period of  $5 \mu\text{s}$ ; averaged over 500 ns windows (5 oscillations). The arrow in (b) indicates the phase measurement in Fig. 2(a). Parameters of the experiment as in Fig. 2.

This is different from Ref. [16], where chimeras appear only for a fraction of the initializations. Figure 4(a) shows the distribution of transient times, where each dot corresponds to the normalized number of transients of  $T_N$  within a certain interval. We find that  $T_N$  follows an exponential distribution (shown as a solid line) according to

$$\rho_N(T_N) = \langle T_N \rangle^{-1} \exp(-T_N / \langle T_N \rangle), \quad (4)$$

with the average transient time  $\langle T_{128} \rangle = 5.4$  min as indicated in the figure. The exponential distribution follows analytically by considering the collapse to synchronization as a Poisson process, which occurs continuously in time at a constant average synchronization rate  $\lambda$  with

$$\langle T_N \rangle = 1/\lambda. \quad (5)$$

The exponential distribution has been found theoretically to describe the transient times for chimera states in the

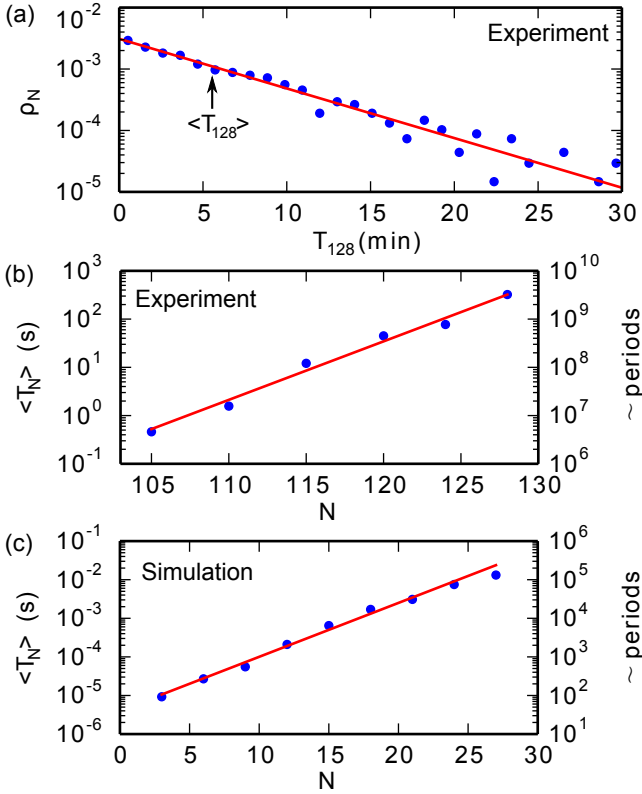


FIG. 4. (a) Histogram of transient times  $T_{128}$  measured from 1000 experimental acquisitions (circles) and distribution function Eq. (4) (solid line). (b), (c) Average transient time  $\langle T_N \rangle$  as a function of  $N$  measured from (b) 1000 experimental transients each, (c) 200 simulated transients each (circles). Both are fitted with Eq. (6) (solid line) with (b)  $\kappa = 0.28 \pm 0.10$ , (c)  $\kappa = 0.30 \pm 0.08$ . The right axis shows the approximate number of periods per transient. Experimental parameters  $R/N \approx 0.24$ ,  $\omega_0 \approx 1000/[19.7 + 2.9 \cdot R]$  (see [29]),  $\bar{\sigma} = \sigma\omega_0^2/\pi$  with  $\sigma = 0.515 \pm 0.018$  ns, initial conditions as in Fig. 2. Numerical parameters are  $R/N = 1/3$ ,  $\bar{\sigma} = 0.089$  MHz  $\cdot$  40/ $R$  (to adjust for the change in coupling range),  $\alpha = 0.1$  and initial conditions as in Fig. 5.  $N$  in (c) is limited by available computation time.

Kuramoto model under the assumption of identical oscillators with symmetric coupling [5]. The appearance of the same scaling is surprising because our experiment has heterogeneity and shows chimeras only for a fraction of the time, which are properties not included in previous models.

We measure the average transient time  $\langle T_N \rangle$  for networks of different size  $N$ , *i.e.*, the number of nodes changes but the network topology is the same. Figure 4(b) shows  $\langle T_N \rangle$  for six different network sizes from  $N = 105$  to  $N = 128$ . The average transient time  $\langle T_N \rangle$  follows approximately an exponential scaling over three orders of magnitude according to

$$\langle T_N \rangle \propto \exp(\kappa N), \quad (6)$$

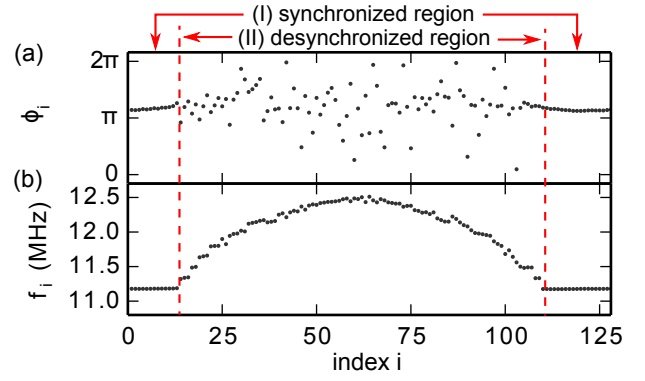


FIG. 5. (a) Phases  $\phi_i$  and (b) frequencies  $f_i = \langle \dot{\phi}_i \rangle / (2\pi)$  of the network at  $t = 50 \mu\text{s}$ . Dynamics are obtained from numerical simulation of Eq. (3) with  $N = 128$ ,  $R = 42$ ,  $\omega_0 = 2\pi \cdot 9.3$  MHz,  $\bar{\sigma} = 2\pi \cdot 0.089$  MHz,  $\alpha = 0.1$ . Dynamics are initialized as in Ref. [2] with  $\phi_i = 6p \exp(-0.76x^2)$ , where  $p$  is a uniform random variable on  $[-0.5, 0.5]$  and  $x = 2\pi i/N - \pi$ . For simplicity, we do not assume frequency heterogeneity and noise in the model. To improve simulation performance, we simulate an altered version of Eq. (3) with a continuous XOR function given by  $\{\tanh[-c \sin(\phi_j) \sin(\phi_i + \alpha)] + 1\} / 2$  with slope  $c = 4$  instead of  $|\Theta[\sin(\phi_j)] - \Theta[\sin(\phi_i + \alpha)]|$ .

with  $\kappa = 0.28 \pm 0.10$  shown with a solid line. Using Eqs. (5) and (6), the synchronization rate

$$\lambda \propto \exp(-\kappa N) \propto V^{-\kappa} \quad (7)$$

follows a power law of the network state-space volume  $V = (2\pi)^N$ , which is plausible [assuming for a single oscillator's phase-space volume  $V = 2\pi$  in accordance with Eq. (3)]. Equation (7) also holds when oscillators have a different finite dimension. This super-transient scaling holds for many spatially-extended systems [32] and also for networks, such as neural networks [11] and Kuramoto oscillators [5]. Therefore, we conjecture that Eq. (7) may be a general law for networks under certain conditions, such as that nodes are nearly identical and that a stable synchronized state exists.

Next, we study the network dynamics numerically using the simplified model in Eq. (3). Figure 5, which is analogous to Fig. 2, shows the dynamics in phase and frequency representations. We use a different coupling range of  $R = 42$  ( $R/N \approx 1/3$ ) than in the experiment because the value used in the experiment ( $R = 30$ ) does not lead to chimera states in the simulation. The figure shows a chimera state with co-existence of a synchronized and desynchronized domains (see also the explanation for Fig. 2). The model also reproduces the characteristic scaling of the transient of Eq. (6), as shown in Fig. 4(c) with  $\kappa = 0.30 \pm 0.08$ , which is analogous to Fig. 4(b). Both results suggest that the model is well suited to describe the experiment qualitatively.

The model is, however, only a first step towards a complete theoretical description of the experimental dynam-

ics because of several differences. First, the simulation shows chimera states for the entire transient [29]. A second difference is that the simulation (the experiment) collapses to a synchronized state (nearly synchronized state), where nodes are phase and frequency synchronized (nearly frequency synchronized but not phase synchronized) after the transient [29]. Third, chimera states appear in different parameter regions in model and experiment.

These differences may be caused by heterogeneity in the experiment  $\alpha_{ij} \neq \text{const}$ , while  $\alpha_{ij} = \text{const}$  is assumed in the model. Specifically, the experiment implements heterogeneous wiring leading to differences in link delays [29]. Further more, differences may be caused by noise and frequency heterogeneity of 0.3%, and transmission delays along the links ( $< 5$  ns) in the experiment.

Theoretical models do not show the observed alternations between chimera states and unsynchronized states. Future work has to fill this gap to uncover the underlying mechanisms.

The Boolean phase oscillator has an important application as a phase-locked loop with multiple inputs. It can be used to realize heavily connected clock networks, which can be expected to be more robust against failure.

In conclusion, we study a network of Boolean phase oscillators that approximately follows equations similar to the Kuramoto model [1]. Large experimental networks of up to 128 non-locally coupled Boolean phase oscillators show complex dynamics, where chimera states of synchronized and desynchronized domains disappear and reappear, which is not yet theoretically understood. The dynamics collapses to a synchronized state after a long transient time, which follows an exponential scaling with the network size as previous predicted in Kuramoto oscillators and neuronal systems [5, 11].

## ACKNOWLEDGMENTS

The authors gratefully acknowledge financial support by the U.S. Army Research Office within Grant W911NF-12-1-0099. D.P.R. and E.S. acknowledge the DFG for financial support in the framework of SFB910. D.R. acknowledges Fondation Supélec for financial support. D.P.R. thanks Philipp Hövel for helpful discussions.

---

[1] Y. Kuramoto and D. Battogtokh, *Nonlin. Phen. in Complex Sys.* **5**, 380 (2002).

[2] D. M. Abrams and S. H. Strogatz, *Phys. Rev. Lett.* **93**, 174102 (2004).

[3] D. M. Abrams, R. Mirollo, S. H. Strogatz, and D. A. Wiley, *Phys. Rev. Lett.* **101**, 084103 (2008).

[4] O. E. Omel'chenko, M. Wolfrum, and Y. L. Maistrenko, *Phys. Rev. E* **81**, 065201(R) (2010).

[5] M. Wolfrum and O. E. Omel'chenko, *Phys. Rev. E* **84**, 015201 (2011).

[6] I. Omelchenko, Y. Maistrenko, P. Hövel, and E. Schöll, *Phys. Rev. Lett.* **106**, 234102 (2011).

[7] A. Zakharova, M. Kapeller, and E. Schöll, *Phys. Rev. Lett.* **112**, 154101 (2014).

[8] I. Omelchenko, O. E. Omel'chenko, P. Hövel, and E. Schöll, *Phys. Rev. Lett.* **110**, 224101 (2013).

[9] M. J. Panaggio and D. M. Abrams, "Chimera states: Coexistence of coherence and incoherence in networks of coupled oscillators," arXiv:1403.6204 (2014).

[10] A. Zumdieck, M. Timme, T. Geisel, and F. Wolf, *Phys. Rev. Lett.* **93**, 244103 (2004).

[11] R. Zillmer, N. Brunel, and D. Hansel, *Phys. Rev. E* **79**, 031909 (2009).

[12] A. Hagerstrom, T. E. Murphy, R. Roy, P. Hövel, I. Omelchenko, and E. Schöll, *Nature. Phys.* **8**, 658 (2012).

[13] M. R. Tinsley, S. Nkomo, and K. Showalter, *Nature. Phys.* **8**, 662 (2012).

[14] E. A. Martens, S. Thutupalli, A. Fourrière, and O. Hallatschek, *Proc. Natl. Acad. Sci. U.S.A.* **110**, 10563 (2013).

[15] L. Larger, B. Penkovsky, and Y. L. Maistrenko, *Phys. Rev. Lett.* **111**, 054103 (2013).

[16] M. Wickramasinghe and I. Z. Kiss, *PloS one* **8**, e80586 (2013).

[17] L. Schmidt, K. Schönleber, K. Krischer, and V. Garcia-Morales, *Chaos* **24**, 013102 (2014).

[18] A. E. Motter, M. Gruiz, G. Károlyi, and T. Tél, *Phys. Rev. Lett.* **111**, 194101 (2013).

[19] D. P. Rosin, D. Rontani, D. J. Gauthier, and E. Schöll, *Phys. Rev. Lett.* **110**, 104102 (2013).

[20] D. P. Rosin, D. Rontani, and D. J. Gauthier, *Phys. Rev. E* **87**, 040902(R) (2013).

[21] D. P. Rosin, D. Rontani, D. J. Gauthier, and E. Schöll, *Chaos* **23**, 025102 (2013).

[22] S. A. Kauffman, *J. Theoret. Biol.* **22**, 437 (1969).

[23] M. Ghil and A. Mullhaupt, *J. Stat. Phys.* **41**, 125 (1985).

[24] L. Glass and C. Hill, *Europhys. Lett.* **41**, 599 (1998).

[25] S. R. Al-araji, Z. M. Hussain, and M. A. Al-qutayri, *Digital Phase Lock Loops* (Springer Verlag, New York, NY, 2006).

[26] R. E. Best, *Phase-Locked Loops* (McGraw-Hill, New York, 2003).

[27] H. Kato, *IEEE Trans. Circuits Syst. I* **45**, 98 (1998).

[28] D. P. Rosin, D. Rontani, and D. J. Gauthier, *Phys. Rev. E* **89**, 042907 (2014).

[29] See Supplemental Material at [insert.link](#) for further information.

[30] Y. Kuramoto, *Chemical Oscillations, Waves, and Turbulence* (Springer, New York, 1984).

[31] S. Nkomo, M. R. Tinsley, and K. Showalter, *Phys. Rev. Lett.* **110**, 244102 (2013).

[32] T. Tél and Y.-C. Lai, *Phys. Rep.* **460**, 245 (2008).